Transaction B: Mechanical Engineering
Vol. 17, No. 6, pp. 468–479

Experimental Investigation of Transition on a Plunging Airfoil

M.R. Soltani[1,*] and F. Rasi Marzabadi[1]

Abstract. *Extensive tests were carried out on a section of a wind turbine blade. The effect of reduced frequency on the boundary layer transition point of the model oscillating in plunge has been investigated. The spatial-temporal progressions of the transition point and the state of the unsteady boundary layer were measured using multiple hot-film sensors. The measurements showed that reduced frequency highly affects variations of the transition point and results in a hysteresis loop in the dynamic transition locations. The dominated frequencies of the boundary layer are found to be a function of the reduced frequency and mean angle of attack.*

Keywords: *Boundary layer transition; Plunging; Reduced frequency; Airfoil; Wind turbine.*

INTRODUCTION

In many engineering applications (e.g. helicopters, turbines, compressors), lifting surfaces experience unsteady motion or are perturbed by the unsteady incoming flows [1,2]. Horizontal axis wind turbine rotors experience large, time-dependent variations in the angle of attack as a result of the control input angles, blade flapping, structural response and the wake inflow. In addition, the blade sections encounter substantial periodic variations in local velocity and incident angle [3,4]. Thus the unsteady aerodynamic behavior of the blade sections must be properly understood to enable accurate predictions of the air loads and aero-elastic response of the rotor system [5].

Prediction of the location of the transition point is important, particularly for wind turbine applications that operate at low Re numbers. The laminar/turbulent properties of the flow field have an important influence on skin friction and separation that affect the lift and drag characteristics of the blade significantly. Thus, the design of wind turbine blades requires the prediction and consideration of flow characteristics at the transition area. For most wind turbine rotors with smooth surfaces, TS instability, laminar separation or turbulence contamination, govern the transition location [6].

Oscillating airfoil flows have been studied in the past using multiple hot-films [7,8]. All these studies have focused on pitching airfoils. There exist limited amounts of data available for other types of motion, such as plunging oscillation. Whilst most angle of attack changes that the rotor blades encounter are due to the variations in the flapping and elastic bending of the blade, i.e. plunging type forcing [9], there are some differences between the effects of unsteadiness on the development of the boundary layer of two motions of pitching and plunging. Although the accelerated flow and pressure-gradient-lag effects are the same for both motions, the leading edge jet effect is of the opposite kind, delaying separation for pitching, and promoting it for plunging oscillations [10].

This study addresses some of the most important aspects of the unsteady boundary layer behavior of an airfoil oscillating in plunge at a subsonic regime. The experiments were conducted at a free stream velocity of 30 m/sec, corresponding to the Reynolds number of 0.42×10^6, and at an oscillation amplitude of ± 8 cm. This investigation involves the effect of reduced frequency on the boundary layer and on the transition point of the airfoil at low to moderate angles of attack. Note that in a plunging motion, the

1. *Department of Aerospace Engineering, Sharif University of Technology, Tehran, P.O. Box 11155-8639, Iran.*
*. *Corresponding author. E-mail: msoltani@sharif.edu*

Received 3 May 2010; received in revised form 22 August 2010; accepted 18 September 2010

model moves vertically up and down inside the tunnel test section. Therefore, only a pure angle of attack plays an effective role, and the pitch rate effect due to the pitching motion is isolated from the problem. Measurement of the surface pressure distribution on this model and the corresponding aerodynamic loads in the plunging motion has been conducted before [11-13]. In this experiment, the effect of reduced frequency (the most important parameter in unsteady motions) on the transition behavior of the model is investigated.

EXPERIMENTAL APPARATUS

The experiments were conducted in a subsonic wind tunnel in Iran. It is of a closed return type, has a test section of 80 cm × 80 cm × 200 cm and operates at speeds from 10 to 100 m/sec. The inlet of the tunnel has a 7:1 contraction ratio with four large anti-turbulence screens and a honeycomb in its settling chamber to reduce tunnel turbulence to less than 0.1 percent in the test section.

The model has 25 cm chord and 80 cm span and is the critical section of a 660 kW turbine blade under construction in Iran. The hot-films that were used are a special version of the flush-mounting DANTEC probe; glue-on type. The sensor is deposited on a Kapton$^{\mathrm{TM}}$ foil with a thickness of about 50 μm. Its sensor is connected to a gold-plated lead area. Eight hot-films were located along the chord at an angle of 20 degrees with respect to the model span to minimize disturbances from upstream one (Figure 1). The position of each sensor on the model is given in Table 1. Data are obtained using a Constant Temperature Anemometer (CTA). All CTA data was transferred to the computer through a 64 channel, 12-bit Analog-to-Digital (A/D)

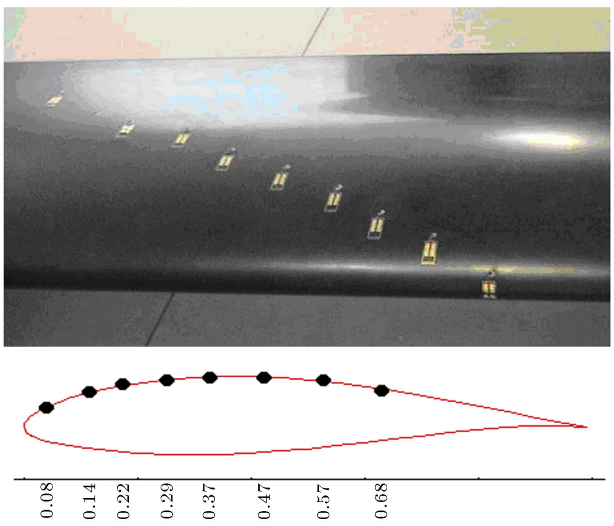

Figure 1. Model along with the location of the hot films.

Table 1. Location of the hot film sensors.

Hot Film	Location (x/c)
s_1	0.08
s_2	0.14
s_3	0.22
s_4	0.29
s_5	0.37
s_6	0.47
s_7	0.57
s_8	0.68

board, capable of an acquisition rate of up to 1200 kHz.

Raw data were then digitally filtered by a low-pass filtering routine. During the filtering process, the cut off frequency was obtained using power spectrum estimation or frequency domain analysis. In this method, the noise that dominates the signal in the time domain appears only as a single peak or spike in the frequency domain. Once the noise frequency is determined, it can be filtered, and a clean signal is then obtained. Figure 2 shows an example of the spectrum of the white noise for one of the hot film channels, which identifies the cut off frequency. From this figure, the cut off frequency is found to be about 150 Hz.

No calibration of the hot film sensors was performed, as the objective of this experiment was to document the qualitative behavior of the boundary layer characteristics. The heat transfer or the voltage output level of the hot film sensor gives a direct recognition of the state of the boundary layer over it. However, the signal magnitude of each sensor was normalized, with respect to its corresponding offset voltage.

The plunging system for the present experiments incorporates a crankshaft to convert the circular motion of the motor to the reciprocal motion, which is transferred to the model by means of rods (Figure 3). The pitch rotation point is fixed at about the wing quarter chord. The plunging displacement was varied sinusoidally as:

$$h = \overline{h}\sin(\omega t).$$

Dynamic tests were performed over a range of reduced frequencies, $k = 0.05 - 0.11$, which are the effective reduced frequencies for this section of the wind turbine blade when operating in the field. The static angles of attack were varied from -5 to 23 degrees.

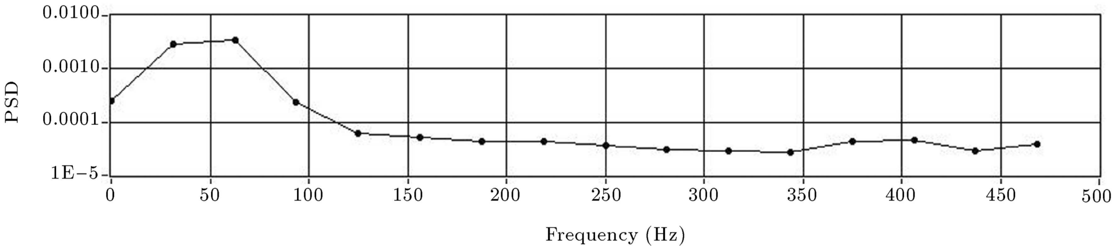

Figure 2. PSD of the white noise for one channel.

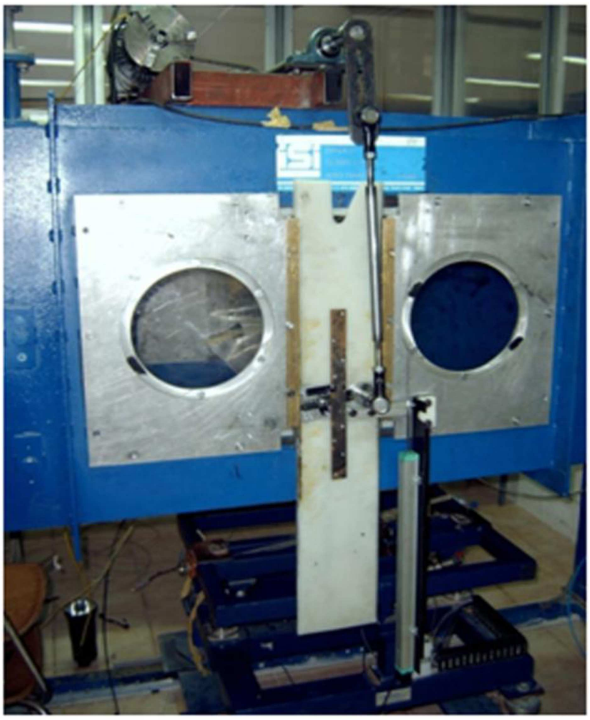

Figure 3. Plunging oscillation system.

RESULTS AND DISCUSSION

To identify the transition point on the airfoil, experiments were carried out at both static and dynamic testing in plunging mode with eight hot film sensors. In the dynamic tests, the effects of reduced frequency on the transition point were studied. The results of the static tests are presented first followed by the dynamic oscillatory data.

Static Tests

Figure 4 shows hot film time histories that illustrate the effects of angle of attack on the surface flow phenomena at a Reynolds number of 0.42×10^6. The designated letters, s_1 through s_8, shown on the left side of each trace are the hot films response in increasing order of chord wise positions, from about 8 to 68 percent of the chord (Table 1). As shown in this figure, at three angles of attack of -5, 0 and 5 degrees, the flow is turbulent only for hot film no. s_8, while for the rest of the films no sign of turbulent flow is seen. This is because for laminar flow the heat transfer is low, thus the hot film sensor gives low output voltage and the corresponding response is smooth with time, as characterized by s_1 through s_7 channels shown in Figures 4a to 4c. However, turbulent flow is associated with high heat transfer, high output voltage and noisy response, as seen from channel s_8 shown in Figures 4a to 4c. By increasing the angle of attack, disturbances appear in other sensors and move upstream toward the leading edge. Eventually, at high angles of attack, all signals except the first channel, s_1, become completely turbulent (Figure 4h). For angle of attack, $\alpha > 10^0$, the flow over the sensors in the vicinity of the trailing edge seems to be separated. For separated flow, the heat transfer varies over a wide range, indicated by the large response fluctuations.

Figure 5 shows the static pressure distribution around the airfoil at various angles of attack for predicting the transition point. The model used for the static and dynamic pressure studies has 64 pressure ports located around its surface; details about the conditions of these tests can be found in [11-13]. Because only eight hot film sensors were glued along the chord of the present model (Figure 1), the position of the transition point could not be specified accurately just from the hot film responses. For example, as explained in Figure 4, the turbulent flow is appeared for hot film no. s_8 at three angles of attack of -5, 0 and 5 degrees, but it is not evident where, on the surface, the flow transits to turbulent. From the surface pressure distribution of Figure 5a, the transition location can almost be estimated, which is marked by the arrows on the graph. A sudden change in the slope of the pressure distribution indicates the transition to turbulent through a separation bubble. The transition points for three other different angles of attack are also shown by the arrows in Figure 5b. The separation bubble moves toward the leading edge with increasing the angle of attack.

The movement of the transition position corresponding to various angles of attack at a chord Reynolds number of 0.42×10^6 is shown in Figure 6. The data is compared to the results of the Eppler [14]

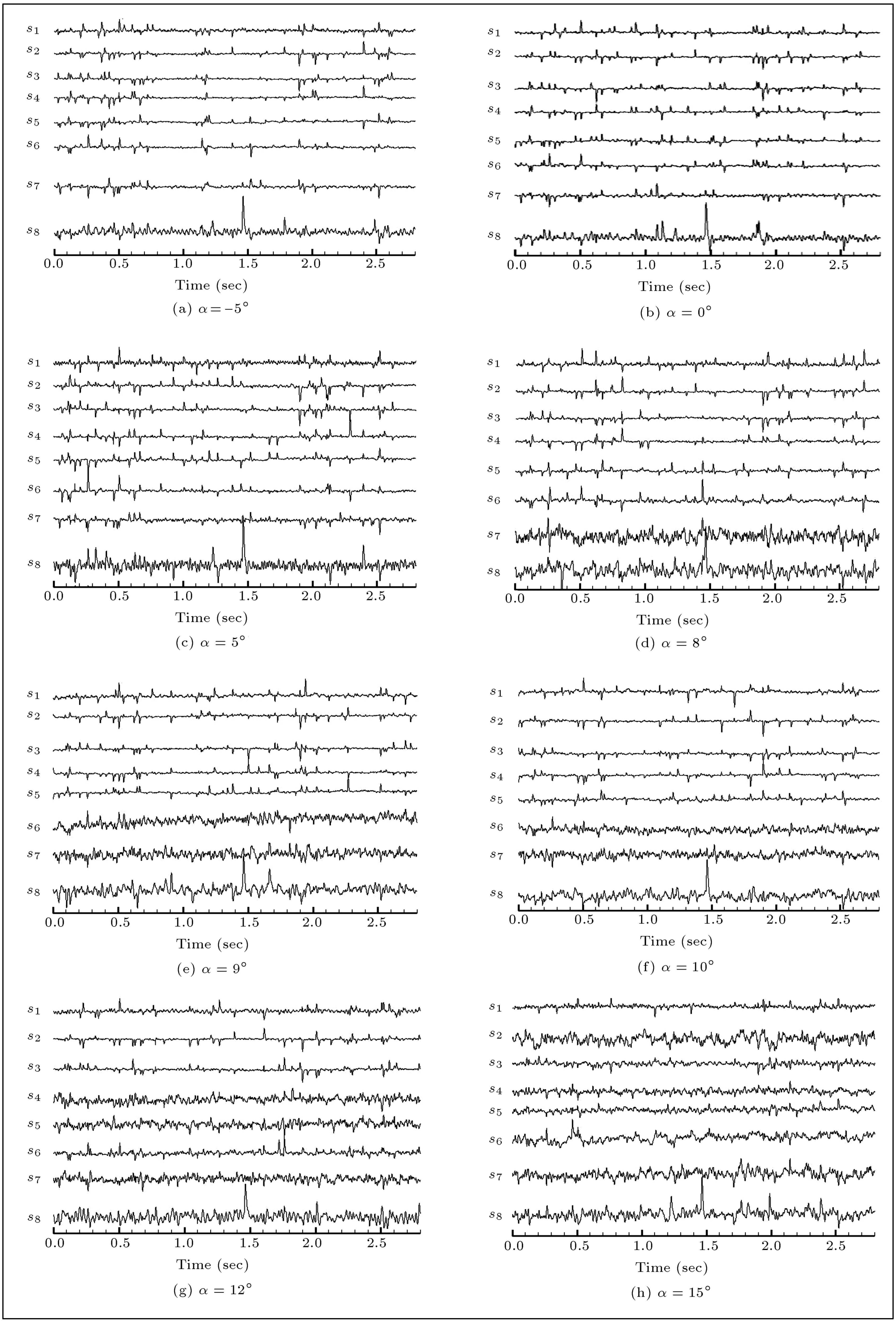

Figure 4. Variations of the hot film response with time.

and the Xfoil [15] codes. Note that the predicted transition points by the Eppler and Xfoil programs for both codes were run for free transition options. It is evident that variations of the transition point with angle of attack for all three methods are similar. However, the differences in the values are probably due to a few differences between the experimental conditions and the terms of these codes. In addition, the transition point estimated from the surface pressure data does not include the length of the separation bubble. As seen from Figures 5a and 5b, the arrows that indicate the transition point are located at the beginning of the separation bubble, while in reality, the flow becomes turbulent at a distance aft of the location of the separation bubble. This distance along with the length of the separation bubble is not considered in our data. Therefore, it is believed that part of the differences between our data and those predicted by the two engineering codes are due to the above phenomenon. At ten degree angles of attack, the Eppler code indicates that the flow is turbulent over the entire airfoil upper surface. However, the results of the Xfoil code and the present experimental data show that there exists a small region in the vicinity of the airfoil leading-edge where the flow is still laminar (Figure 6).

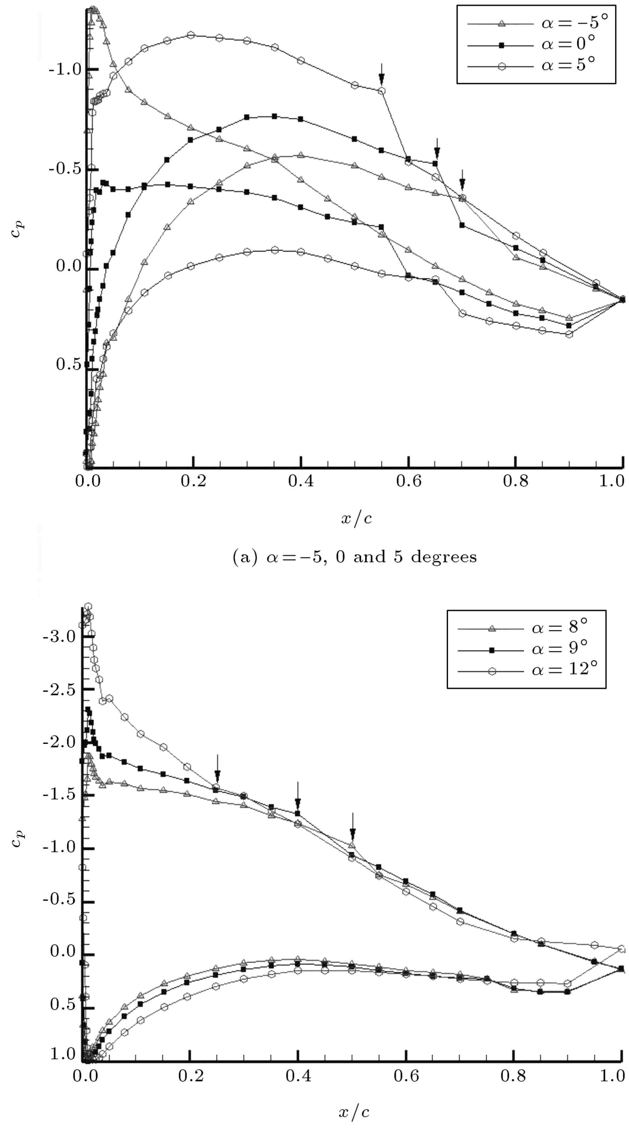

(a) $\alpha = -5$, 0 and 5 degrees

(b) α = 8, 9 and 12 degrees

Figure 5. Static surface pressure distribution at various angles of attack.

Dynamic Tests

All dynamic experiments were conducted at a Reynolds number of 0.42×10^6 and for oscillation amplitude of $\pm$ 8 cm. Data for three different reduced frequencies of $k = 0.05$, 0.08 and 0.11 are presented in this paper. The model was set to mean angles of attack of 5, 10 and 18 degrees, which correspond to the regions before, around and beyond the static stall angle of attack of the airfoil, respectively. The static stall angle of attack for this particular airfoil is about 11 degrees [11-13].

It should be noted that in the plunging motion, the plunging displacement can be transformed into the equivalent angle of attack using the potential flow transformation formula, $\overline{\alpha}_{\text{eq}} = ik\overline{h}$, where $\overline{\alpha}_{\text{eq}}$ is in radians, and $\overline{h}$, the plunging amplitude, has been nondimensionalized with respect to the model semi-chord. The mean angle of attack is, of course, added to the equivalent angle [16]. From the above transformation formula, the effect of plunging motion on the induced angle of attack is evident. As the plunging amplitude or the reduced frequency increases,

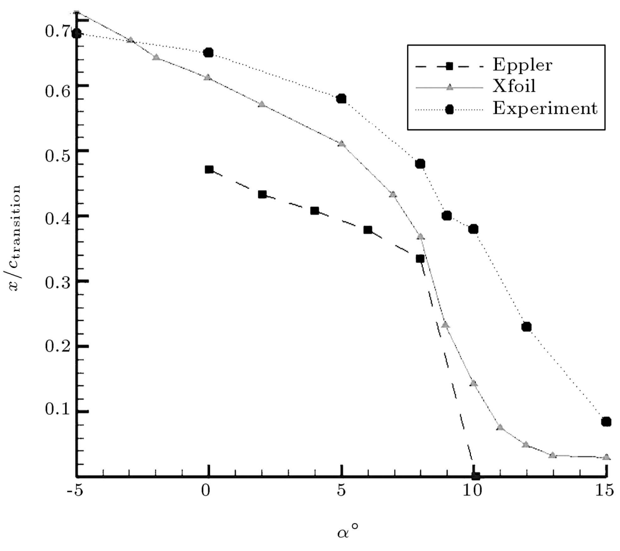

Figure 6. Comparison of the measured transition point with the present engineering codes.

the values of the induced angle of attack increase too. The airfoil plunges sinusoidally with time, hence the corresponding induced angle of attack, which is due to the oscillation time history effects on the vertical motion of the model, is 90 degrees out of phase, with respect to the plunging motion (Figure 7). Thus, when $h = 0$ during the down stroke portion of the plunging motion, this is equal to the maximum angle of attack of the model, while in the upstroke one, the reverse is true, the minimum angle of attack is reached.

Figures 8 through 10 show composite plots of time traces of the hot film sensors glued on the upper surface of the airfoil oscillated below, within and beyond the static stall angle of attack. The sensor numbers are shown on the left side of these figures. Variations of the plunging displacement and the corresponding angle of attack with time for all cases are shown on the top of the figures. The y-axis represents the normalized voltage output of each sensor.

In Figure 8, the model is set to an angle of attack

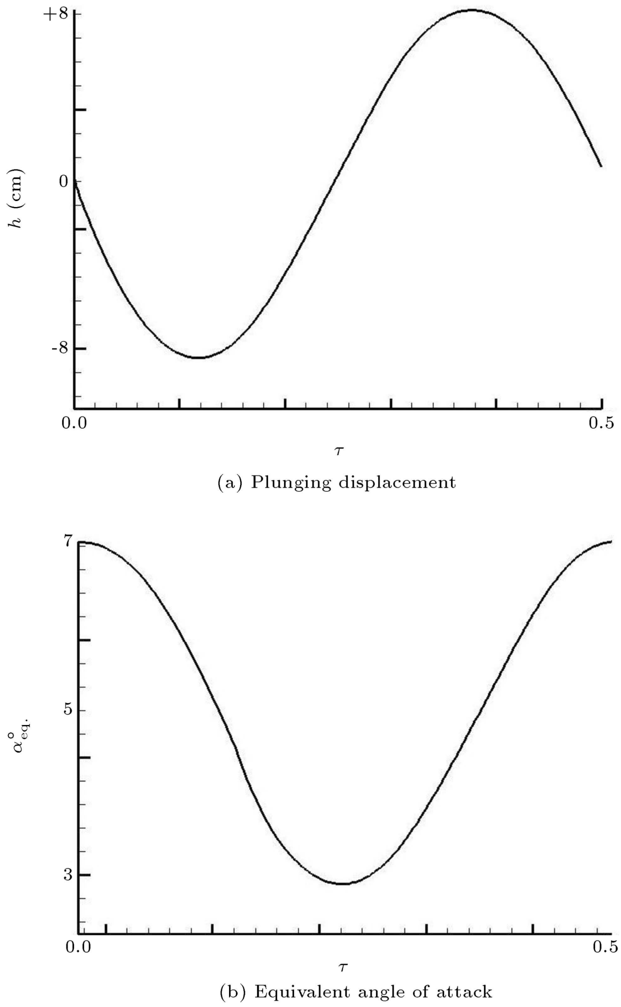

Figure 7. Time history of the plunging motion and its corresponding equivalent angle of attack.

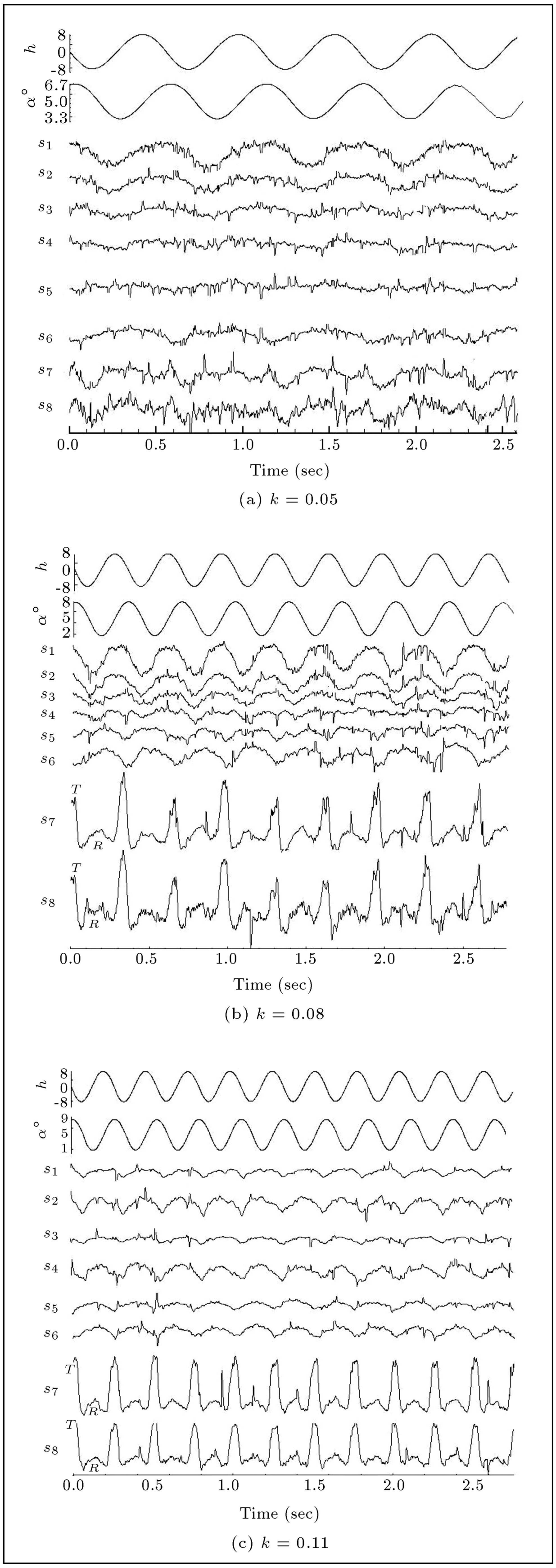

Figure 8. Variations of the voltages with time, $\alpha_0 = 5°$.

of 5 degrees. In this case, the maximum equivalent angle of attack is less than the static stall angle. As seen for all reduced frequencies, the output signals of channel 1, s_1, to channel 6, s_6, do not show significant perturbation and have a smooth response with time. Therefore, the flow is laminar through the entire oscillation cycle in this region (from the leading edge to $x/c \approx 0.5$). The output signals of channels s_1 to s_4 follow variations of the equivalent angle of attack. However, the outputs of channels s_5 and s_6 that are located after the maximum thickness of this model ($x/c = 0.35$) show a phase difference with respect to the variations of the equivalent angle of attack, due to effect of the pressure gradient outside the boundary layer. The flow at the last two channels, s_7 and s_8, have a combination of laminar-turbulent flow. For the lowest reduced frequency case, the equivalent angle of attack varies between 3.3 and 6.7 degrees (Figure 8). It is seen from Figure 6 that, in the static case for these variations of angles of attack, the transition point is located approximately at $x/c \approx 0.6$ and $x/c \approx 0.52$, respectively. Since, for $k = 0.05$ the last two channels are dominated by the turbulent flows, where the intensity of the fluctuations are relatively high and there is no obvious sign of transition, it is expected that the locations of transition and relaminarization are relatively the same as the static case for both upstroke and down stroke motions. For the two higher reduced frequency cases (Figures 8b and 8c), there is an indication of transition in the output signals of channels s_7 and s_8. It can be seen that as the equivalent angle of attack increases, transition to turbulent flow occurs (indicated by symbol 'T' in Figures 8b and 8c), and the output of the sensor shows a corresponding increase in the magnitude of the signal, as well as an increase in the fluctuation amplitude. As the equivalent angle of attack decreases, the flow again becomes laminar (indicated by symbol 'R'). Similar to the static case, the transition point moves toward the leading edge with increasing the angle of attack, and can be traced from the outputs of channels s_7 and s_8, in one oscillation cycle.

In Figure 9, the model is set to a mean angle of attack of 10 degrees, near the static stall angle of attack. For the lowest reduced frequency case, $k = 0.05$, the equivalent angle of attack varies from 8.3° to 11.7°, and for the highest one, $k = 0.11$, the range of angle of attack variations is from 6° to 14°. It is seen that for $k = 0.05$, the output of channels s_1 to s_4 have a smooth response with time and follow the variations of the equivalent angle of attack with some phase differences. Thus the flow is laminar up to near 30% of the chord during the entire oscillation cycles (Figure 9a). It is in contrast to the results of the static tests (Figure 6). As the reduced frequency increases, the laminar flow region is restricted to the leading edge. For $k = 0.08$, channels s_1 to s_3 (Figure 9b), and for $k = 0.11$, only the first two channels show laminar flow (Figure 9c). Close examination of the output voltages indicate that the flow at the last two channels, s_7 and s_8, are separated for all reduced frequencies, since they have a 180 degree phase difference, with respect to the variations of angle of attack, and the response fluctuations are relatively high. As explained in Figure 8, the transition and relaminarization locations can be obtained from the output signals of the channels that show the combination of laminar-turbulent flow. This result will be shown later.

In Figure 10, the model is oscillated in the post stall region, $\alpha_0 = 18^\circ$. It is seen that for all reduced frequencies, there is no laminar flow along the airfoil upper surface. For $k = 0.05$, the output signal of the first channel, s_1, shows turbulent flow, which follows the variations of the angle of attack. However, for $k = 0.08$, the first two channels, and for $k = 0.11$, channels s_1 to s_3 show turbulent flow. It means that the reduced frequency maintains the turbulent flow on the surface of the airfoil near the leading edge. For $k = 0.05$, channels s_2 to s_6 show a combination of the turbulent-separation flow. During one oscillation cycle, when the angle of attack is low, the flow is turbulent; with increasing the angle of attack, it becomes separated. The last two channels show separated flow during the entire cycles with 180 degrees phase difference, with respect to the variations of the angle of attack, and have high fluctuations (Figure 10a). For $k = 0.08$, channels s_3 to s_5 show a combination of the turbulent-separation flow and the other channels, $s_6 - s_8$, show separated flow (Figure 10b). For $k = 0.11$, channels s_6 to s_8 show separated flow, which means that by increasing the reduced frequency, the region of the separated flow near the trailing edge is also increased (Figure 10c).

Figure 11 shows variations of the transition and relaminarization points with angle of attack, for example for the case of $\alpha_0 = 10$ degrees. Static data are provided in the figure for comparison. The directions shown indicate increasing or decreasing the equivalent angle of attack of the model during the plunging motion. As seen from this figure, when compared with the static case, the onset of the unsteady boundary layer transition promotes to the lower effective angles of attack at a given chord wise position, and relaminarization generally occurs at a higher α than that of the transition. Thus there is a hysteresis in the transition-relaminarization cycle that increases with increasing k. This is attributed to the accelerated flow, pressure-gradient-lag and leading-edge jet effects in unsteady motions. As described by Ericson [9], the accelerated flow and pressure-gradient-lag effects are the same for pitching and plunging airfoils. However,

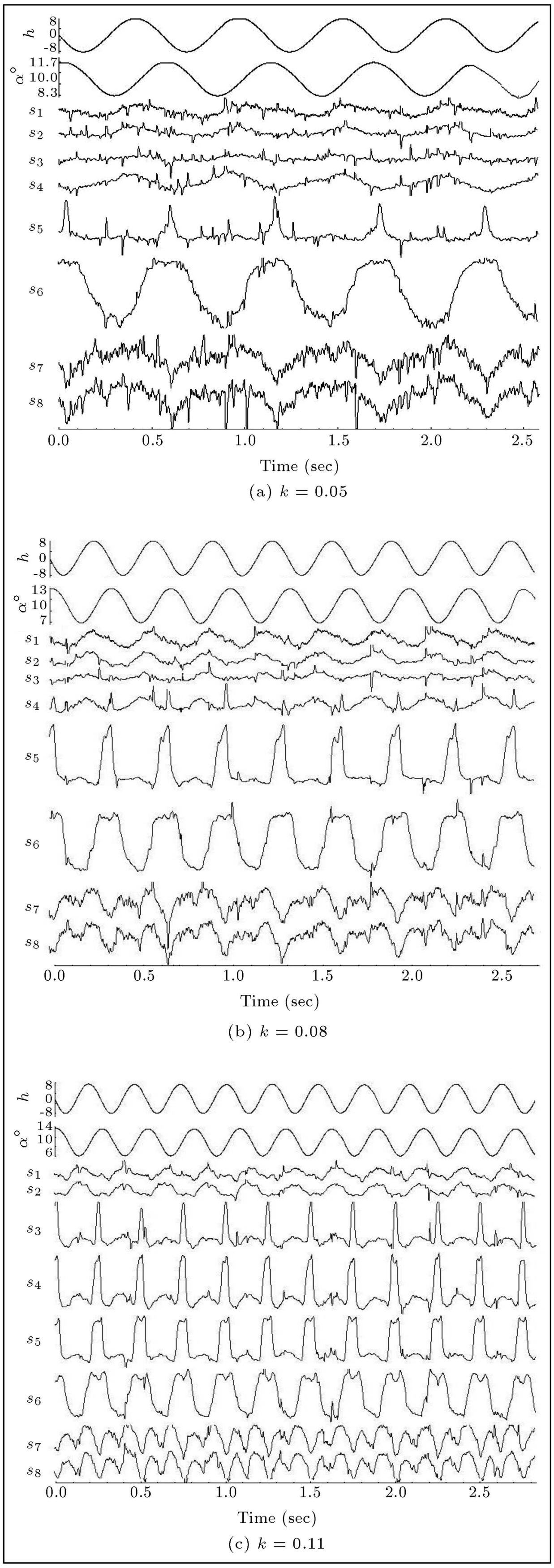

Figure 9. Variations of the voltages with time, $\alpha_0 = 10°$.

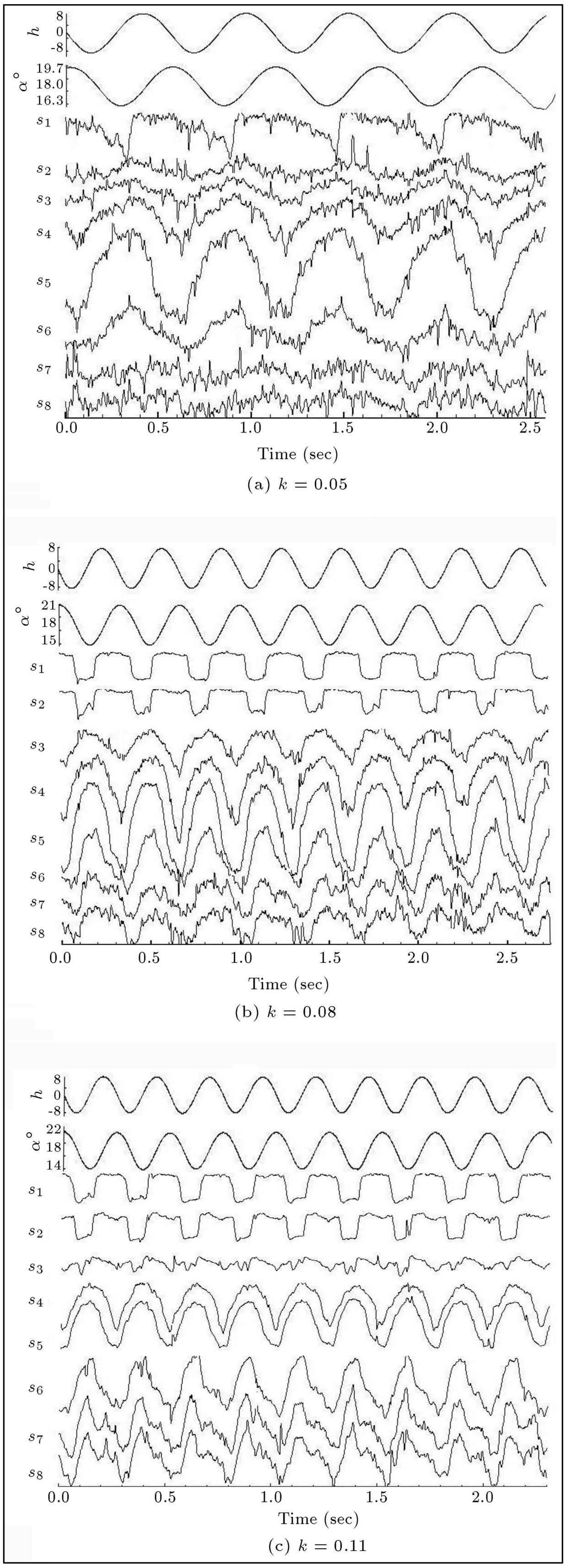

Figure 10. Variations of the voltages with time, $\alpha_0 = 18°$.

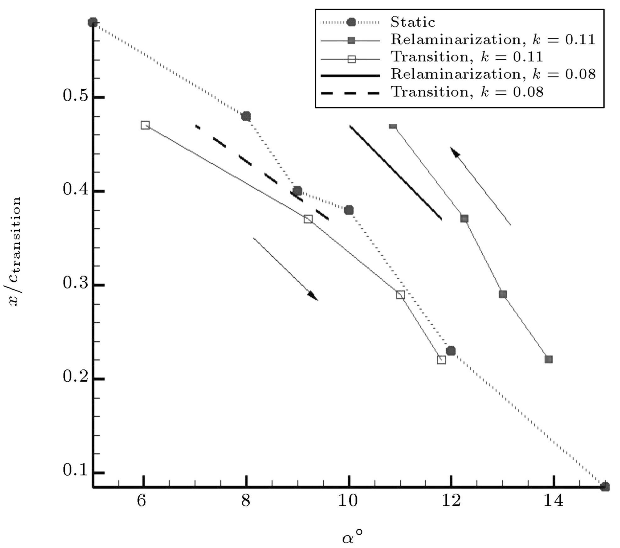

Figure 11. Variations of the onset of boundary layer transition and relaminarization with α and k, $\alpha_0 = 10°$.

the leading-edge jet effect is of the opposite kind, delaying separation for pitching and promoting it for plunging oscillations. According to [9] "For the plunging airfoil the leading-edge jet effect is zero at the mid portion, and reaches peak magnitude at the end portion. The effect is adverse at high angles of attack and favorable at low angles". The adverse moving wall effects for the plunging airfoil are large enough to completely overpower the favorable accelerated flow effects. Thus, the earlier transition would occur for increasing rather than for decreasing effective angles of attack.

Another approach for determining boundary layer characteristics is through the frequency domain analysis. Figure 12 compares the power spectral of the hot film signals at various reduced frequencies. In this figure, the model is set to a mean angle of attack of 10 degrees. The frequencies corresponding to the PSD's peaks are indicated on the top of them in the spectrum plots. In the first two channels, Figures 12a and 12b, it is seen that the amplitudes of the spikes are lower than for the other channels, for all reduced frequencies. This is in agreement with Figure 9, that there is laminar flow in the vicinity of the leading edge for all reduced frequencies. In channel s_3 (Figure 12c) the boundary layer instability frequencies and also the amplitudes of the spikes grow for the case of $k = 0.11$. It means that for this reduced frequency, TS instability frequencies may be present at this location, while for the other two reduced frequencies, $k = 0.05$ and 0.08, the flow is still laminar. The spectrum plots of channels s_4 and s_5 (Figures 12d and 12e) show that for $k = 0.11$, the amplitudes of the spikes grow more and the combination of laminar-turbulent flow is apparent in these locations of the airfoil surface. For $k = 0.08$, the boundary layer instability frequencies are appeared in channel s_5 (Figure 12e), and for the lowest reduced frequency, $k = 0.05$, they are seen in channel s_6 (Figure 12f). In the last two channels (Figures 12g and 12h), it is seen that there are spikes in the lower range of frequencies of the spectrum and they disappear at higher frequency ranges. It means that there is no turbulent flow in this region and, as mentioned in Figure 9, the flow may be separated. In the entire spectrum plots, note that the first frequency of the PSD peak is proportional to the oscillation frequency, e.g. it is increased from $f \approx 1.3$ Hz for $k = 0.05$ to $f \approx 4.3$ Hz for $k = 0.11$. Further, there is a relation between the frequencies of the spikes in all spectrum plots. It seems that they are the coefficients of the oscillation frequency and are amplified when the boundary layer instability grows.

Figure 13 shows the effect of the mean angle of attack on the power spectral of the hot film signals for sensors s_2, s_5 and s_8. The reduced frequency is equal to $k = 0.08$. It is seen that at $x/c = 0.14$, the maximum amplitude of PSD is related to the case of $\alpha_0 = 18°$, and for the other two mean angles of attack, the flow is still laminar (Figure 13a). At a location of $x/c = 37\%$ (Figure 13b), the maximum spikes are related to the case of $\alpha_0 = 10°$, and for the lowest mean angle of attack, the flow is still laminar. However, at a location of x/c=0.68, the maximum amplitude of PSD is for $\alpha_0 = 5°$ and the PSD amplitudes of the other mean angles of attack are reduced, with respect to the PSD of channel s_5. It means that with increasing the mean angle of attack, the appearance of laminar/turbulent spikes or TS instability frequencies move toward the leading edge.

CONCLUSION

Experiments were performed to measure the position of the transition point and the characteristics of the boundary layer in a plunging motion under different conditions. Dynamic tests were conducted at different reduced frequencies and mean angles of attack. The data showed hysteresis between the transition location in the upstroke and down stroke motion. The width of the hysteresis loop varied with the reduced frequency. Boundary layer transition occurred earlier for increasing (rather than for decreasing) the effective angle of attack. The frequency domain analysis of the hot film signals revealed that dominated frequencies of the boundary layer are a function of the reduced frequency and mean angle of attack. For almost all cases examined here, the flow was separated in the vicinity of the airfoil trailing-edge, and the transition locations, as well as the separation region, were a function of the mean angle of attack.

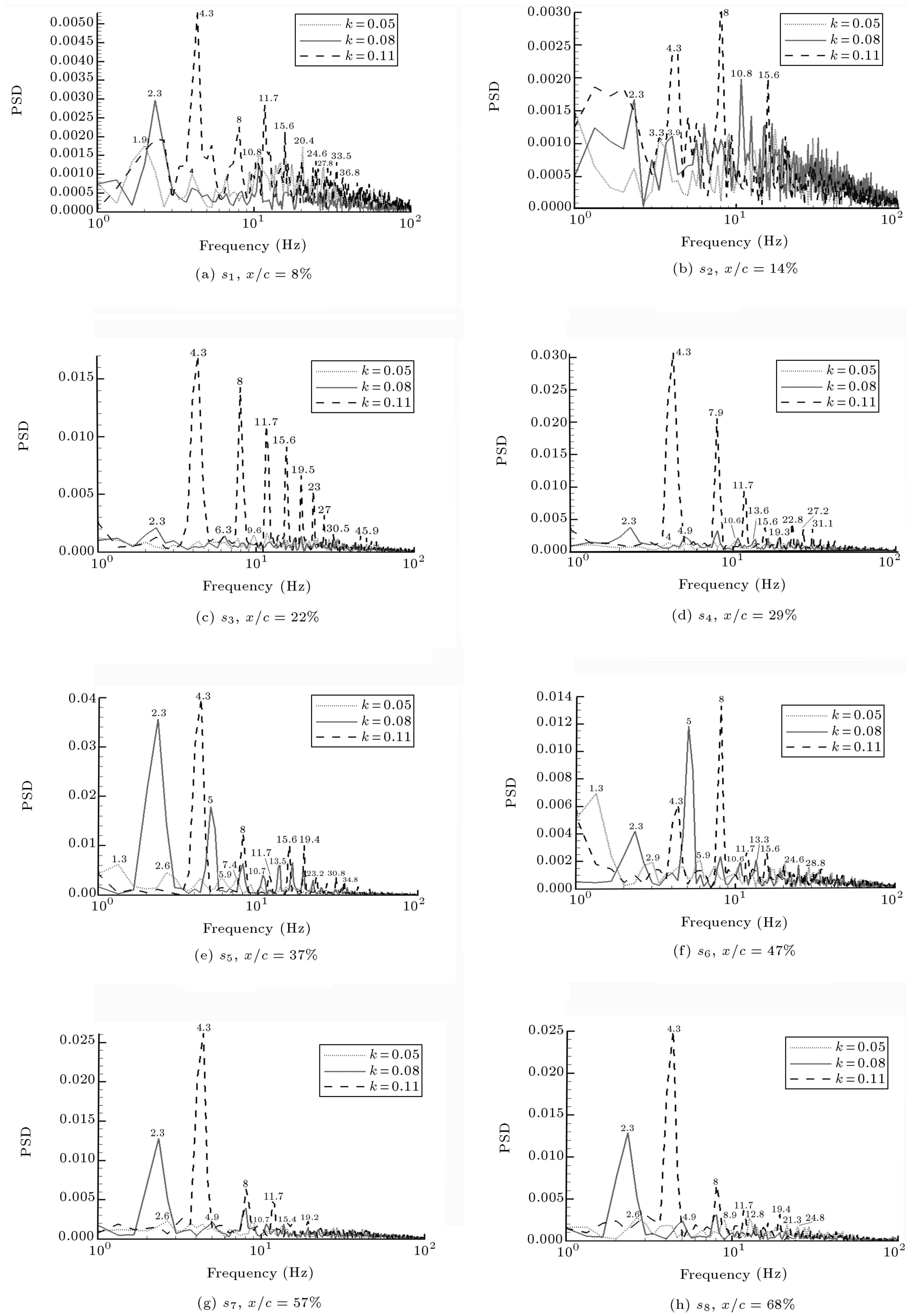

Figure 12. Variations of power spectral of hot film sensors with k, $\alpha_0 = 10°$.

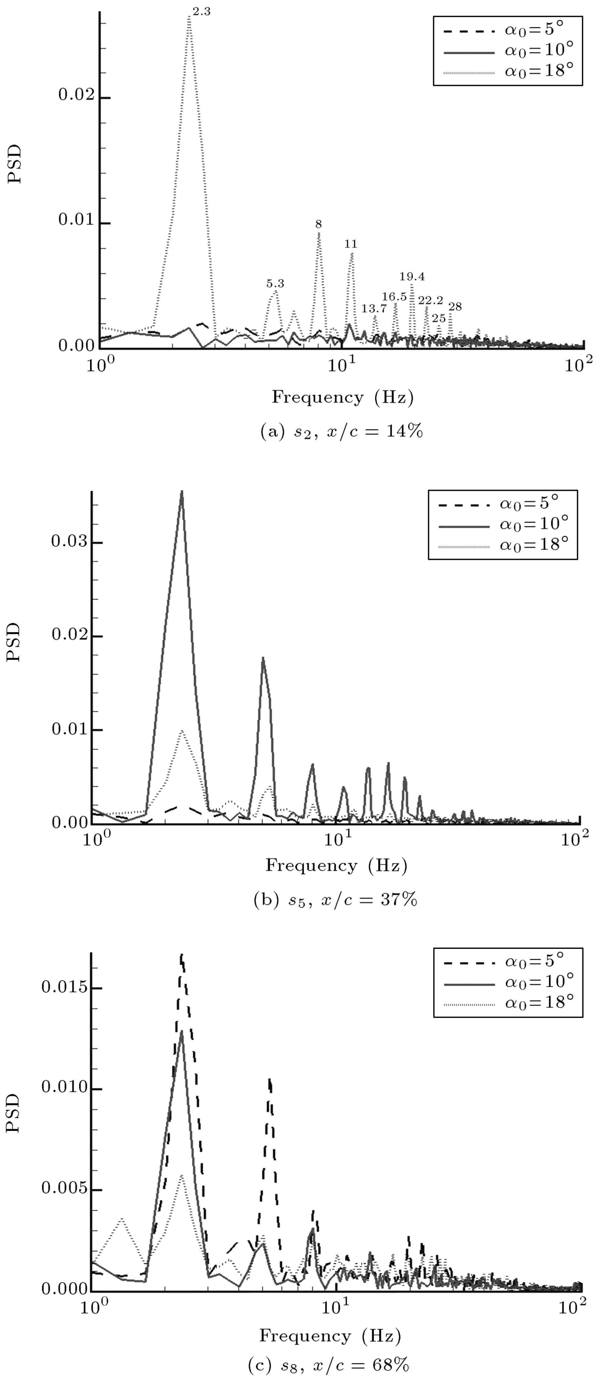

Figure 13. Variations of power spectral of hot film sensors with α_0, $k = 0.08$.

NOMENCLATURE

PSD	power spectral density
TS	tollmien schlichting
c	airfoil chord (cm)
x	distance from the leading edge of the airfoil (cm)
h	plunging displacement (cm)
H	amplitude of the plunging motion (cm)
$\bar{h}$	dimensionless plunging amplitude, $\bar{h} = \frac{2H}{c}$
s	sensor
f	plunging frequency (Hz)
U_∞	free stream velocity (m/sec)
k	reduced frequency, $k = \frac{\pi f c}{U_\infty}$
t	time (sec)
t'	period of oscillation
τ	dimensionless time, $\tau = t/t'$
T	transition
R	relaminarization
α	angle of attack (deg)
α_0	mean incidence angle (deg)
$\bar{\alpha}$	amplitude of the pitching motion (deg)
ω	angular frequency (rad/s)
$()_{\text{eq}}$	equivalent motion

REFERENCES

1. Mccroskey, W.J. "Unsteady airfoils", *Annual Rev. Fluid Mech.*, U.S. Army Aerodynamics Laboratory and NASA, pp. 285-309 (1982).
2. Leishman, J., *Principles of Helicopter Aerodynamics*, Cambridge Press (2000).
3. Huyer, S.A., Simms, D. and Robinson, M.C. "Unsteady aerodynamics associated with a horizontal-axis wind turbine", *AIAA Journal*, **34**(7), pp. 1410-1419 (1996).
4. Robinson, M.C., Galbraith, RAMcD., Shipley, D. and Miller, M. "Unsteady aerodynamics of wind turbines", *Paper 95-0526, 33rd Aerospace Sciences Meeting*, Reno, NV (1995).
5. Leishman, J. "Challenges in modeling the unsteady aerodynamics of wind turbines", *AIAA 2002-0037, 21st ASME Wind Energy Symposium and 40th AIAA Aerospace Sciences Meeting*, Reno, NV (2002).
6. Brodeur, R. and van Dam, C.P. "Transition prediction for a two dimensional Navier-Stokes solver applied to wind-turbine airfoils", AIAA paper 2000-0047 (2000).
7. Chandrasekhara, M.S. and Wilder, M.C. "Heat-flux gauge studies of compressible dynamic stall", *AIAA Journal*, **41**(5), pp. 757-762 (2003).
8. Lee, T. and Basu, S. "Measurement of unsteady boundary layer developed on an oscillating airfoil using multiple hot-film sensors", *Experiments in Fluids*, **25**, pp. 108-117 (1998).
9. Tyler, C.J. and Leishman, J.G. "Analysis of pitch and plunge effects on unsteady airfoil behavior", *Presented at the 47th Annual Forum of the American Helicopter Society* (1991).
10. Ericson, L.E. "Moving wall effects on dynamic stall can be large-fact or fiction", *AIAA-91-0430, 29th Aerospace Sciences Meeting*, Reno, Nevada (1991).

11. Soltani, M.R. and Rasi Marzabadi, F. "Effect of plunging amplitude on the performance of a wind turbine blade section", *The Aeronautical Journal*, **111**(1123), pp. 571-587 (2007).

12. Soltani, M.R. and Rasi Marzabadi, F. "Effect of reduced frequency on the aerodynamic behavior of an airfoil oscillating in a plunging motion", *Journal of Scientica Iranica*, **16**(1), pp. 40-52 (2009).

13. Soltani, M.R., Seddighi, M. and Rasi Marzabadi, F. "Comparison of pitching and plunging effects on the surface pressure variation of a wind turbine blade section", *Journal of Wind Energy*, DOI: 10.1002/we.286 (2008).

14. Eppler, R. and Somers, D.M. "A computer program for the design and analysis of low-speed airfoils", NASA TM 80210 (1980).

15. Drela, M. "An analysis and design system for low Reynolds number airfoil aerodynamics", *Conference on Low Reynolds Number Airfoil Aerodynamics*, University of Notre Dame (1989).

16. Carta, F.A. "A comparison of the pitching and plunging response of an oscillating airfoil", NASA CR-3172 (1979).

BIOGRAPHIES

Mohammad Reza Soltani, a professor in the Aerospace Engineering Department of Sharif University of Technology, Tehran, has a Ph.D. in aerodynamics from the University of Illinois at Urbana-Champaign, USA. His research interests include: Applied Aerodynamics, Unsteady Aerodynamics, Wind Tunnel Testing, Wind Tunnel Design and Data Processing.

Faezeh Rasi Marzabadi received her B.S. degree in Aerospace Engineering from Amirkabir University of Technology in 2003 and her M.S. degree in Aerodynamics from Sharif University of Technology in 2005, where she is now a Ph.D. student in that field. Her research interests are: Applied Aerodynamics, Unsteady Aerodynamics, Wind Tunnel Testing and Data Processing.